WPPFC-CPR(17) 17002

A Weckmann et al.

High-Z Material migration, fuel retention and liner morphology of the TEXTOR tokamak

Preprint of Paper to be submitted for publication in Proceeding of 16th International Conference on Plasma-Facing Materials and Components for Fusion Applications

This work has been carried out within the framework of the EUROfusion Consortium and has received funding from the Euratom research and training programme 2014-2018 under grant agreement No 633053. The views and opinions expressed herein do not necessarily reflect those of the European Commission.

Ageing of structural materials in tokamaks: TEXTOR liner study

A. Weckmann[1]
P. Petersson[1]
M. Rubel[1]
E. Fortuna-Zaleśna[2]
W. Zielinski[2]
E. Grigore[3]
C. Ruset[3]
A. Kreter[4]

[1]*Department of Fusion Plasma Physics, KTH Royal Institute of Technology, 10044 Stockholm, Sweden*
[2]*Faculty of Materials Science and Engineering, Warsaw University of Technology, Warsaw, Poland*
[3]*Plasma Physics and Nuclear Fusion Department, National Institute for Laser, Plasma and Radiation Physics, Bucharest, Romania*
[4]*Forschungszentrum Juelich GmbH, EURATOM Association, 52425 Juelich, Germany*

ABSTRACT

After the final TEXTOR shut-down, all machine parts of this tokamak became accessible for comprehensive studies. This unique chance enabled the study of the Inconel 625 liner by a wide range of methods. The aim was to evaluate eventual alteration of surface and bulk characteristics from recessed wall elements that may influence the machine performance. The surface was covered with stratified layers consisting mainly of boron, carbon, oxygen, and in some cases also silicon. Wall conditioning and limiter materials hence predominantly define deposition on the liner. Deposited layers on recessed wall elements reach micrometre thickness within decades, peel off and may contribute to the dust inventory in tokamaks. Fuel retention was about 4 at% of the overall layers, with no evidence for diffusion into the Inconel substrate. Inconel 625 retained its mechanical strength despite 26 years of cyclic heating, stresses and particle bombardment.

1. INTRODUCTION

Studies of plasma-material interactions (PMI) are for technical reasons restricted to removable wall parts of a tokamak, as for example plasma-facing components (PFCs), such as limiter or divertor parts, or wall probes. Examination of permanent wall structures is normally limited to photographic surveys or sampling of deposits. The final shut-down of the TEXTOR tokamak, a carbon limiter machine operating from 1983 till 2013, has created unique opportunities for research including the structural elements of the machine wall.
In magnetic fusion devices, sub-systems and PFCs are mounted on support structures made from stainless steel or high-performance alloys, so called super alloys. These support structures can be either the vacuum vessel itself or a second shell within the vacuum vessel, which is called a liner. In either case these are long-term components and cannot be readily exchanged upon failure. Although these structural materials are recessed and not magnetically connected with the main plasma, as the PFCs are, they suffer from particle and photon bombardment. In detail, the bombarding species are: (i) charge exchange neutrals, (ii) plasma particles from wall conditioning like boronisation and glow discharge (GD) cleaning, (iii) microscopic particles from PFCs, i.e. dust and droplets, (iv) photons, (v) neutrons. One can thus expect a change of surface morphology and even bulk properties. Neutron irradiation effects are not taken into account in this paper since the neutron doses in TEXTOR were negligible.
Support structures are integrated parts of big vacuum systems, and as such they need to be heated

during pump-down to achieve good vacuum. This “baking”, cyclic heating of large metal structures up to several hundred degrees Celsius, causes thermal fatigue.
As final factor influencing steel properties in magnetic fusion devices are omnipresent hydrogen species. They may lead to hydrogen induced embrittlement, an effect known for metals [CITATION HWi01 \l 1031].
Two points will be addressed in this paper. How is the surface of structural materials altered during their long service time in a magnetic fusion device? What are the mechanical properties of structural materials after decades of cyclic heating and hydrogen exposure? In attempt to answer these questions, a broad range analysis was conducted on samples from the TEXTOR liner, which was in duty for 26 years.

2. METHODS

Samples investigated in this study have been extracted from the TEXTOR tokamak. A general overview of it can be found in [CITATION ONe05 \l 1031]. The liner, which has been studied, was built into the machine during a major shut-down in 1986/7 and is described comprehensively in [CITATION WKo90 \l 1031]. It was needed to accommodate the new Advanced Limiter Test II (ALTII) pump limiter. The liner was fabricated from rolled 1 mm thick Inconel 625, a nickel based super-alloy with high mechanical performance at elevated temperatures. More details are given in [CITATION INC13 \l 1031].
The main limiter of TEXTOR was the ALTII limiter, a pumped belt limiter made of eight toroidal segments armoured with 28 graphite tiles each [CITATION RWC90 \l 1031]. Auxiliary plasma heating took place via neutral beam injection (NBI) [CITATION HEu89 \l 1031], either in co- or counter-direction, and ion cyclotron resonance heating (ICRH) [CITATION WKo90 \l 1031]. Other systems of relevance in this paper were glow discharge (GD) antennae and the limiter lock 1 (LL1) for insertion of test limiters [CITATION BSc05 \l 1031]. A map of all mentioned sub-systems is given in Figure 1.
Samples were cut from the liner by a circular saw, to a size in the order of 100-300 cm^2. These samples were extracted from six different areas to assess the influence of sub-systems on the liner: a) close to LL1 where various materials were tested and impurities were injected, b) close to one ICRH antenna, c) close to the co-NBI port to check for influence of NBI heating on surrounding wall surfaces, d) close to one GD antenna. Two more samples were taken from distinct areas on the basis of visual inspection: e) deposition area with grainy appearance, f) deposition area with green peeling layers. Every part of the liner had an individual appearance and hence no effort was taken to seek for a “reference”. Sample backsides were examined as well. The sampling positions are marked in Figure 1.
Surface analysis was conducted with several techniques. Optical microscopy was used to get a first impression of the surface appearance. Ion beam analysis (IBA) of different kinds was used to probe the surface: elastic recoil detection analysis (ERDA) with time-of-flight (ToF) system to analyse elemental composition for the top 500 nm [CITATION PSt16 \l 1031], and nuclear reaction analysis (NRA) to analyse the deuterium depth profile down to ca. 10 µm. Electron beam analysis was used to obtain pictures of surface morphology, and to probe elemental composition in particular points on the surface: scanning electron microscopy (SEM), energy dispersive X-ray spectroscopy (EDX), scanning transmission electron microscopy (STEM) in connection with focused ion beam (FIB) sample preparation. Glow discharge optical emission spectroscopy (GDOES) probed elemental composition down to several tens of micrometres. Tactile profilometry was used to obtain surface topology. Mechanical stress-strain testing was performed to assess mechanical properties.

3. RESULTS AND DISCUSSION

This section is divided into five parts. First, results about surface appearance and topology will be given, i.e. microscopy and profilometry results. Then the surface compositions at the various sample locations obtained by ToF-ERDA and EDS are presented. Sub-surface analysis results, i.e. below the first few micrometres, from GDOES and STEM are addressed thereafter, followed by outcomes about fuel retention. The section closes with results from mechanical testing.
The plasma current under normal configuration went counter-clockwise when seen from the top of TEXTOR, see Fig. 1. Positions towards the plasma current with respect to a certain object is called "upstream", while the "leeward" side of an object with respect to the plasma current is called "downstream". Please notice that the notation "upstream" and "downstream" applies in the same manner to the toroidal flow at the plasma edge [CITATION Tam95 \l 1031].

3.1 SURFACE APPEARANCE AND TOPOLOGY

Optical and electronic microscopy reveals a highly diverse surface appearance, see Fig. 2. Upstream of the test limiter, where experiments with material testing and impurity seeding took place, one can see stratified layers with tendency for peeling, see Figure 2a. Despite the peeling tendency the roughness is the lowest of all samples, see Table 1. Downstream of the test limiter we see thick layers with very rough, scaly appearance, see Fig. 2b. This may be due to test limiter erosion, with subsequent deposition of the eroded carbon on the downstream side. Also the sample from the ICRH antenna vicinity shows thick, flaky layers. Downstream at the NBI port one can see bubble formation, both in microscopic pictures and in topological profiles, see Figure 2c. Topographical maps and roughnesses are shown in Fig. 3 and Table 1, respectively.

Table 1: Roughnesses of six probed samples – R_a arithmetic mean roughness, R_q quadratic mean roughness, R_max maximum deviation from mean.

Sample position	**R_a [µm]**	**R_q [µm]**	**R_max [µm]**
LL1 (upstream)	0,1	0,2	2,3
ICRH antenna	0,8	1,0	5,9
NBI port (downstream)	0,7	1,0	5,5
GD antenna	0,2	0,3	3,0
Green peeling layer (e)	0,4	0,7	4,6
Grainy depositions (f)	0,8	1,1	7,5

Overall, scaly and flaky appearance with evidence of deposits fragmentation (1-100 µm flakes) is found on most analysed samples, see Fig. 2d. It indicates that deposition on recessed wall elements like the liner may be considerable dust sources. In section 3.2 it will be found that 18% silicon in a certain region is found with ToF-ERDA, although this layer is buried beyond the reach of this technique. Assuming that hence these 18% are only seen due to peeled-off layers, one could hence expect the respective fraction of surface area to be converted to dust. The area of the liner is roughly 37,7 m^2 [CITATION WKo90 \l 1031], disregarding the port holes. Subtracting the area of the main PFCs, ca. 12,1 m^2 in total [CITATION RWC90 \l 1031][CITATION BGi97 \l 1031], yields 25,6 m^2. 18% thereof would correspond to a "peeling area" of 4,6 m^2, which has to be scaled down to account for the port holes and the fact that not every area may exhibit such a high peel-off. A conservative approach with 1 m^2 "peeling area" and 1 µm of layer thickness (for layer thickness see end of section 3.2) yields 1 cm^3 of dust, or about 2 g with carbon and boron as two main

constituents (see section 3.2). Peeling layers partly covered in deposits suggest that dust generation by exfoliation has been ongoing for a longer time and the given estimate may be seen as a lower boundary.

3.2 SURFACE COMPOSITION AND LAYERING

ToF ERDA was performed to analyse the overall surface composition of the topmost 500 nm. Its results are used to assess the average composition of the top layers. STEM results thereafter will show the layered structures and their composition in higher detail than ToF ERDA could. An example for ToF ERDA spectra and depth profile is given in Fig. 4.
Boron is the most common element at the plasma-facing surface, followed by carbon and oxygen. Together they compose about 85-90% of the deposited layers, with on average 60% boron, 14% carbon and 11% oxygen over all layers. As will be seen in Section 3.4, deuterium is at fourth position in the most common element ranking. The remaining few percent in that surface layer are made of silicon, Inconel components and nitrogen. Only *per mille* amounts are attributed to species like tungsten or molybdenum. Fluorine as constituent from tracer gas injection, i.e. from hexafluorides, was also found within the *per mille* range, usually two to three times more than molybdenum. Very much silicon, almost 18% of the whole layer, was found at a deposition area with grainy appearance (Fig. 1e, Fig. 2d). Especially high content of Inconel was found upstream of the NBI port samples (Fig. 1c), which can be either attributed to the bare liner substrate below peeled-off layers, or to deposition. It cannot be excluded that this is actually copper from the NBI dump plates, since the mass resolution of ToF ERDA is not sufficient to distinguish between e.g. nickel - the main constituent of Inconel 625 - and copper. Elemental composition found with ToF ERDA is listed in Table 2.

Table 2: Deposited elements on different liner samples as found with ToF ERDA in at%. D was omitted.

Sample position	**B**	**C**	**O**	**Inconel**	**Si**	**N**	**Mo**
LL1 upstream	67.6	14.2	5.0	1.6	-	0.8	0.2
LL1 downstream	55.6	24.4	9.6	0.3	0.2	0.8	0.2
ICRH antenna	59.1	15.5	15.6	1.1	0.6	1.6	0.1
NBI upstream	41.8	10.4	34.8	6.7	1.3	1.2	0.1
NBI downstream	67.4	7.5	8.7	1.7	3.5	1.0	0.1
GD antenna	70.9	9.6	4.7	2.7	0.1	1.1	0.1
Green peeling layer (e)	68.7	17.0	3.4	0.1	-	0.2	-
Grainy deposits (f)	50.4	10.4	7.5	1.5	0.2	1.4	-
Average	**60.2**	**13.6**	**11.2**	**2.0**	**0.7**	**1.0**	**0.1**

EDX performed during electron microscopy on a subset of samples confirmed boron, carbon and oxygen as main constituents, with traces of Inconel metals in the low percent range, and molybdenum and tungsten (used in tracer experiments [CITATION MRu13 \l 1031][CITATION AWe16 \l 1031]) in the *per mille* range. The small amount of Inconel metals detected by EDX proves that the deposited thickness exceeded 1 µm and no signal from the substrate was recorded. ToF ERDA on the backside of the samples, i.e. the liner side facing the vacuum vessel instead of the plasma, revealed thinner deposition layers at all positions, usually 250-400 nm. Main

constituents were boron, oxygen, carbon and silicon, representing on average 41%, 31%, 10% and 8% of the layers, respectively. This shows that wall conditioning with boronisation and siliconisation coated also the liner backside. A much higher fraction of Inconel constituents was found in the layers, namely on average 5% or 2,5 times more than on the inside. It is possible that due to surface roughness the substrate signal was recorded together with the deposition layers. At one position close to the test limiter, 12% of the layer consisted of lithium, in total about $4{,}8 \cdot 10^{17}$ /cm^2. The only possible source for this element on that position is the lithium beam diagnostic described in [CITATION GAn08 \l 1031].
The liner backsides show much smoother coatings than on the liner inside, see Fig. 5a, but in some cases also on the backside indications for flaking could be found. A particular sample close to the co-NBI exhibited only 50 nm thick layers and revealed a very corroded metal surface, see Fig. 5b.

Vertical FIB cuts from a few samples for STEM exhibit a large potential of analysing PWI and deposition history by deposited layer “archaeology”. In the following, different deposited elements will be tested for correlation between their signals as a measure for co-deposition. In such way one can check whether the migration of one element possibly triggered the migration of another. Measure for correlation is the Pearson Correlation Coefficient (PCC) as defined in [CITATION Bro06 \l 1031], with PPC = 1 meaning perfect correlation, PPC = -1 meaning perfect anti-correlation, and PPC = 0 meaning no correlation.
The first example is displayed in Fig. 6 and will now be discussed in detail, followed by other cuts from other locations. The cut we discuss first was taken from the deposition area with grainy appearance that featured high silicon content, see text above and Figure 2d. It exhibits a regularly layered structure of mainly boron, carbon and oxygen with very distinct concentration variations. Carbon and boron correlate strongly with each other, with PCC of 0,95 throughout the whole layer. This is possibly due to erosion and subsequent deposition of boronised carbon limiters. Oxygen shows an anti-correlation to carbon and boron in the first 2 µm, but correlates further down, see Figure 5. Silicon is deposited in two deposition bands, the first in 2,0-2,8 µm depth, the second in 3,0-3,5 µm depth. Exfoliation seen in Fig. 2d exposed parts of the silicon layer and made it detectable even for ERDA, see text above. The depth profiles of boron, carbon, oxygen and silicon are shown in Fig. 7.
All probed Inconel metals – nickel, iron, chromium, manganese and niobium – correlate with each other, with PCCs ranging between 0,4 for trace metals niobium and manganese and 0,9 for main constituents nickel and iron. However, these metals do not correlate significantly¿) with boron and carbon, nor with oxygen. Hence, increased flux of Inconel metals does not increase the erosion of limiters.
Depth profiles from two other STEM analysed places, close to the test limiter (a) and to one ICRH antenna (b), have been analysed as well (areas a and b in Fig. 1). Close to the test limiter and the ICRH antenna the oxygen signal correlates with boron and carbon, contrary to the sample analysed above. As before, good correlation between boron and carbon is found at all depths. All three samples show good correlation (PCC ~ 0,8-0,9) between Inconel metals nickel, chromium, iron and molybdenum, up to the topmost layer. Hence, most molybdenum deposition on the liner is from previous liner erosion, not from molybdenum limiter experiments, e.g. [CITATION AKr07 \l 1031], or molybdenum hexafluoride tracer injection [CITATION AWe16 \l 1031]. For the purely extrinsic element tungsten, no significant correlation could be found with other metals or carbon and oxygen. Hence, tungsten introduced into TEXTOR did not cause major sputtering of either limiters or liner. This finding is in line with previous observations [CITATION MRu97 \l 1031].
Layer thicknesses found from FIB cuts and in GDOES measurements scatter between about 0,5 µm to several micrometres. The maximum thickness was found close to the ICRH antenna (b) with 3,88 µm, followed by the grainy layer in Fig. 2d with 3,65 µm .On some samples the thickness differs by a factor of two between two analysed points a few centimetres apart. This shows that deposition on the liner can be highly inhomogeneous in terms of incoming particle flux, although all analysed samples were oriented head-on to the plasma.

3.3 ANALYSIS OF SUB-SURFACE LAYERS

Previously mentioned TEM analysis showed grain sizes in the order of several μm. This is in accordance with values found in the literature for 1 mm thick Inconel 625 plates [CITATION ZPa10 \l 1031]. Inconel composition was analysed with GDOES and compared to a reference Inconel 625 piece. Values from around 12 μm depth were taken where the elemental signals saturated. In shallower depth, surface roughness effects obscured the real composition. Five elements present in Inconel 625 were analysed in every sample and could be compared: nickel, chromium, molybdenum, iron, cobalt. We see a depletion of molybdenum and iron with respect to the reference, and a higher concentration for nickel and chromium. Only cobalt levels are very constant in each and every sample. Details are listed in Table 3. The obtained values are largely in agreement with [CITATION ZPa10 \l 1031], except for iron.

Table 3: Inconel composition – comparison of all probed Inconel 625 species.

Sample name	Ni	Fe	Cr	Co	Mo
(a) point 1 (down)	60	1,2	20	0,1	7,4
(a) point 2 (down)	66	1,4	23	0,1	8,6
(d) point 1	68	1,3	22	0,1	8,3
(d) point 2	68	1,4	22	0,1	8,5
(d) point 3	66	1,3	21	0,1	8,2
(e)	68	1,3	21	0,1	8,7
Average	**66**	**1,3**	**21,5**	**0,1**	**8,3**
Reference	64	3,2	19,7	0,1	12

3.4 FUEL RETENTION

Deuterium content was measured with NRA, utilising a He-3 beam at 2,8 MeV. Deuterium is depleted in the first 500 nm, has its maximum deposition at around 1-2 μm, contributing up to 10,5% to the overall atomic concentration at that depth. Depth profiles are shown in Fig. 8. Highest concentrations are found at the test limiter (Area a), one ICRH antenna (Area b) and the co-NBI port (Area c) where bubbles were found with microscopy, see Figure 2c. Very low deuterium amounts are found close to a GD antenna due to fuel removal via GD cleaning. Table 4 shows the maximum and average fuel content in the layers as well as the overall areal density. Deuterium depth profiles of each sample are shown in Figure 6. Samples close to LL1, the NBI port and the ICRH antenna exhibit a qualitatively similar deuterium depth profile: Gaussian with a peak at around 1 μm depth and a FWHM around 1-1,4 μm. The FWHM is of the order of two times the arithmetic mean roughness, see Table 1. Since the layer thickness is of the order of 1 μm, most deuterium seems to peak at the deposition-substrate interface, with the profile broadened by surface roughness effects. Samples with peeling layers and grainy deposits (Areas e and f) show more homogeneous deuterium deposition, possibly due to fuel retention in consecutively built-up layers of several μm thickness. Deuterium content is very low and shallow near to the GD antenna due to thin layers and the purging effect of glow discharges. No deuterium was found beyond about 4 μm,

indicating that no diffusion far into the Inconel has occurred. The detection limit for deuterium for this kind of analysis is about 300 ppm.
Assuming that the deuterium is mainly stored in the deposited layers and the layer-liner interface, we can estimate the fuel retention of the liner throughout its lifetime. Average areal density is $1{,}2 \cdot 10^{18}$ /cm^2. As calculated above the liner area is about 25,6 m^2, disregarding port holes. Multiplied with the areal density we obtain an overall fuel retention of ca. $3{,}1 \cdot 10^{23}$ deuterium atoms, or about 1 g of deuterium on the whole liner. The liner backside exhibits much lower deuterium content, about one tenth of the plasma-facing side, all of which is deposited in the topmost 2 µm.

Table 4: Basic data about fuel retention in liner samples.

Sample name	**Areal concentration [1E17/cm2]**	**Average D fraction of layer [%]**	**Maximum D fraction in layer [%]**
(a) upstream	10.6	6.2	10.5
(a) downstream	16.8	5.3	7.8
(b)	17.3	6.9	9.0
(c) upstream	7.0	3.6	5.1
(c) downstream	15.7	6.8	10.3
(d)	0.8	0.4	0.6
(e)	14.8	4.4	4.3
(f)	14.0	3.8	5.3
Average	**12,1**	**4.7**	**6.6**

3.5 MECHANICAL STRENGTH

The following mechanical properties were tested with three different samples from three different locations, i.e. with nine samples in total: elastic modulus E, yield strength YS, tensile strength TS, and modulus of rupture R. E is the resistance of a material to be pulled apart; YS defines the force per area that it needed to start plastic deformation; TS is the maximum force per area a material can bear before failure; R measures the resistance to bending. A proper definition of all these characteristics can be found for instance in [CITATION WFH05 \l 1053]. Table 5 shows the respective values obtained from all measured samples, plus the literature values found in [CITATION INC13 \l 1031]. It can be seen that the liner Inconel performs within the material range given by [CITATION INC13 \l 1053], and slightly below the values given in [CITATION www17 \l 1031]. In comparison, the maximum stress expected on the liner were 150 Mpa [CITATION WKo90 \l 1031]. For 350°C, YS of Inconel 625 is estimated to be around 250 Mpa both in [CITATION INC13 \l 1031] and [CITATION WKo90 \l 1031]. Combining the expected maximum stress results and the mechanical testing results after the limiter's lifetime, one can conclude that the limiter operated below its maximum capabilities and did hence not suffer any noticeable mechanical degradation.

Table 5: Mechanical properties of nine samples from three liner parts.

Sample	E [GPa]	YS [MPa]	TS [MPa]	R [MPa]
(a) 1	212	434	892	677

(a) 2	222	431	889	698
(a) 3	210	428	887	712
(b) 1	219	429	881	674
(b) 2	222	432	882	740
(b) 3	230	432	887	645
(f) 1	206	427	879	719
(f) 2	152	428	878	736
(f) 3	203	427	882	726
Average	**208**	**430**	**884**	**703**
Literature at 350°C	208 * 207 # ~190*	414-758 * 517 # ~250*	827-1103 * 930 # ~820*	780* ~700*

* taken from [CITATION INC13 \l 1031]
# taken from [CITATION www17 \l 1031]

4. CONCLUSION

For the first time, a comprehensive examination was conducted for the liner, a permanent not replaceable wall component after 26 years of duty time, mostly at elevated temperature in the range 200-350 ºC. As it could be expected after such long operation period the deposition on the liner is highly inhomogeneous regarding the structure and composition and thickness of the layers. Their thickness in the range of micrometres is judged to be fairly small. Parts of these layers peel off, forming flakes with 1-100 μm size and may hence contribute to the overall dust production from recessed areas. Surface roughness is in the micrometre range due to flaking, and in one case close to the co-NBI due to bubble formation. Taking this into account it is therefore difficult to assess how many layers peeled-off during the operation period. Deposition layers on the liner consist mainly of boron, carbon and oxygen, with substantial silicon fraction in deeper layers. This is due to wall conditioning and erosion of limiter species. Boron and carbon are co-deposited. Wall conditioning also influenced the backside of the limiter. Medium-Z metals around iron are co-deposited and are hence believed to come from liner erosion. Depth profiles of neither Inconel metals nor tungsten used in PWI and transport experiments correlate with boron and carbon depth profiles. An important point is low fuel retention; on average about 4,7% of the total layer composition. It is also stressed that no clear sign of fuel diffusion into the liner have been found. The Inconel 625 retained its mechanical strength after 26 years of operation under thermal cycling, particle bombardment and mechanical stress due to mounted components, induced currents and thermal expansion. In summary, detailed analyses of the liner have allowed to complete the study of all internal wall components after decommissioning of the TEXTOR tokamak.

ACKNOWLEDGEMENTS

We are grateful to Thomas Krings for liner sample removal. This work has been carried out within the framework of the EUROfusion Consortium and has received funding from the Euratom research and training programme 2014-2018 under grant agreement No 633053. The views and opinions expressed herein do not necessarily reflect those of the European Commission. The work has been partly funded by the Swedish Research Council (VR) through contracts no. 621-2012-4148 and 2015-04844. All ion beam analysis was conducted in the Ion Technology Centre, Uppsala University, Sweden and is therefore highly acknowledged.

[1] H. Wipf, ”Solubility and diffusion of hydrogen in pure metals and alloys,” *Physica Scripta,* vol. T94, 2001.

[2] O. Neubauer, G. Czymek, B. Giesen, P. W. Hüttemann, M. Sauer, W. Schalt och J. Schruff, ”Design features of the TEXTOR tokamak,” *Fusion Science and Technology,* vol. 47, pp. 76-86, 2005.

[3] W. Kohlhaas, C. Stickelmann, B. Brandt och F. Durodie, ”New liner and ICRH antennae; Integration of ALT-II in TEXTOR,” *Fusion Engineering and Design,* vol. 13, pp. 321-336, 1990.

[4] ”INCONEL (R) alloy 625,” Special Metals Corporation, 2013. [Online]. Available: www.specialmetals.com/documents/Inconel alloy 625.pdf. [Använd 2017].

[5] R. W. Conn, K. H. Dippel, W. B. Gauster och A. Miyahara, ”The toroidal belt pump limiter, ALT-II, in the TEXTOR tokamak,” *Fusion Engineering and Design,* vol. 13, pp. 251-259, 1990.

[6] H. Euringer, M. Lochter, U. Pfister och R. Uhlemann, ”Neutral injection for TEXTOR,” *Fusion Engineering Proceedings,* pp. 991-995, 1989.

[7] B. Schweer, S. Brezinsek, H. G. Esser, A. Huber, P. Mertens, S. Musso, V. Philipps, A. Pospieszczyk, U. Samm, G. Sergienko och P. Wienhold, ”Limiter lock system at TEXTOR: flexible tools for plasma-wall investigation,” *Fusion Science and Technology,* vol. 47, pp. 138-145, 2005.

[8] P. Ström, P. Petersson, M. Rubel och G. Possnert, ”A combined segmented anode gas ionization chamber and time-of-flight detector for heavy ion elastic recoil detection analysis,” *Review of Scientific Instruments,* vol. 87, 2016.

[9] H. F. Tammen, ”The ion velocity distribution of tokamak plasmas: Rutherford scattering at TEXTOR,” Utrecht, 1995, pp. 106-109.

[10] B. Giesen, H. Bohn, W. Huettemann, O. Neubauer, M. Poier och W. Schalt, ”Technical lay-out of the dynamic ergodic divertor,” *Fusion Engineering and Design,* vol. 37, pp. 341-346, 1997.

[11] M. Rubel, J. Coenen, D. Ivanova, S. Möller, P. Petersson, S. Brezinsek, A. Kreter, V. Philipps, A. Pospieszczyk och B. Schweer, ”Tungsten migration studies by controlled injection of volatile compounds,” *Journal of Nuclear Materials,* vol. 438, pp. 170-174, 2013.

[12] A. Weckmann, P. Petersson, M. Rubel, P. Wienhold, S. Breyinsek, J. W. Coenen, A. Kirschner och A. Pospieszczyk, ”Local migration studies of high-Z metals in the TEXTOR tokamak,” *Physica Scripta,* vol. T167, 2016.

[13] G. Anda, D. Dunai, G. Petravich, J. Sárközi, S. Zoletnik, B. Schweer, T. Baross, I. G. Kiss och B. Mészáros, ”First Measurements with the re-installed accelerated Lithium beam diagnostics on TEXTOR,” i *35th EPS Conference on Plasma Physics*, Hersonissos, 2008.

[14] Bronstein, Semendjajew, Musiol och Mühlig, Taschenbuch der Mathematik, Frankfurt am Main: Verlag Harri Deutsch, 2005, 2006.

[15] A. Kreter, P. Wienhold, D. Borodin, S. Brezinsek, S. Droste, T. Hirai, A. Kirschner, A. Litnovski, V. Philipps, A. Pospieszczyk, U. Samm, O. Schmitz och G. Sergienko, ”Study of local carbon transport on graphite, tungsten and molybdenum test limiters in TEXTOR by 13CH4 tracer injection,” *Journal of Nuclear Materials,* Vol. %1 av %2363-365, pp. 179-183, 2007.

[16] M. Rubel, V. Philipps, U. Kögler, T. Tanabe, D. Larsson, B. Unterberg, A. Pospieszczyk, Y. Ueda och P. Wienhold, ”Impact of molybdenum and tungsten test limiters on ion fluxes in the plasma edge of TEXTOR,” *Journal of Nuclear Materials,* vol. 249, pp. 116-120, 1997.

[17] Z. Pakiela, ”Microstructure and mechanical properties of Inconel 625 superalloy,” *Obróbka Plastyczna Metali,* vol. 21, pp. 143-154, 2010.

[18] W. F. Hosford, Mechanical behaviour of materials, Cambridge University Press, 2005.
[19] ”www.espimetals.com,” 2017. [Online]. Available: www.espimetals.com/index.php/technical-data/89-inconel-625. [Använd 2017].

Figure 1: TEXTOR with PFCs – ALTII limiter (black), inner bumper limiter (grey), poloidal limiter (black striped) – and sub-systems. Sampled areas (red hatched) are labelled (a) to (f).

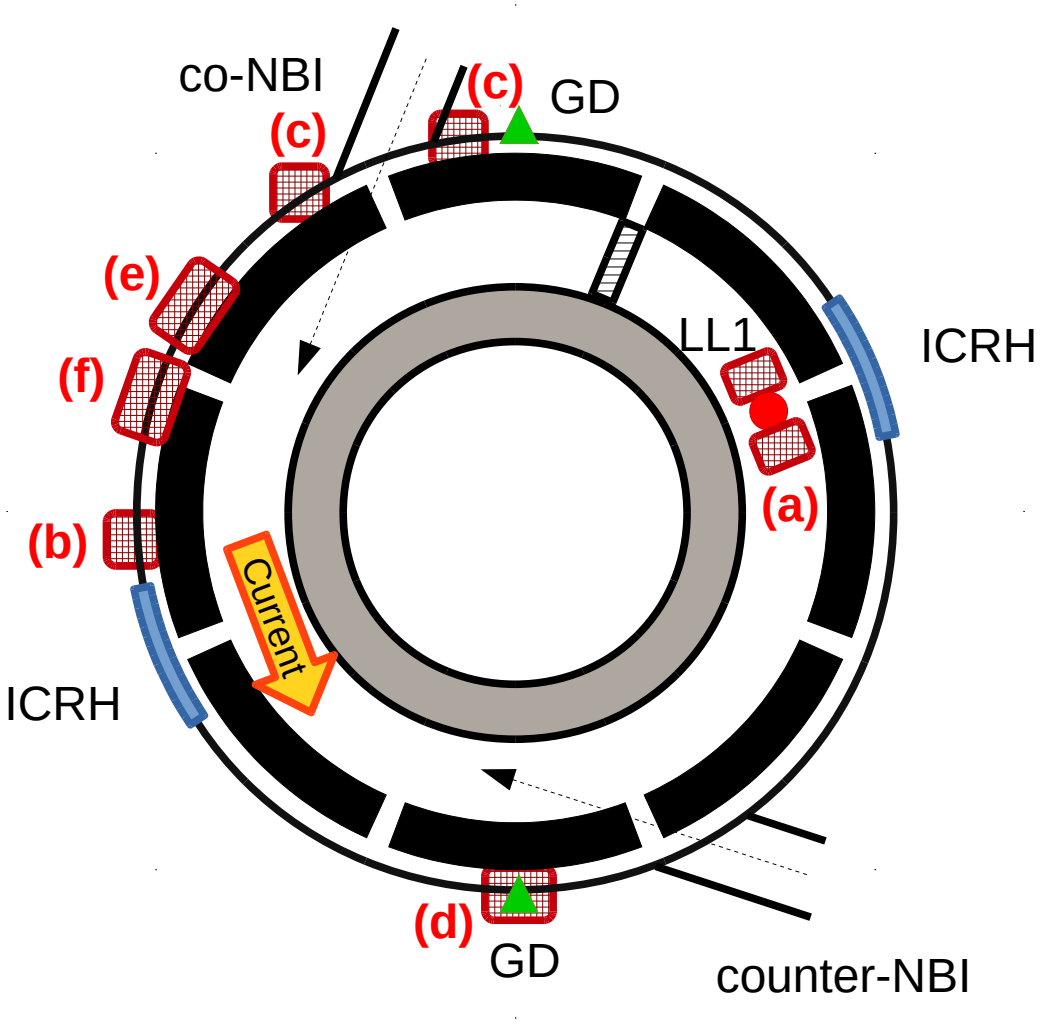

Figure 2: Deposition at LL1 – a) upstream, b) downstream; c) bubbles downstream of the co-NBI port; d) peeling layers at Position (f) in Figure 1. Images were obtained with optical microscopy (a, b) and SEM (c, d).

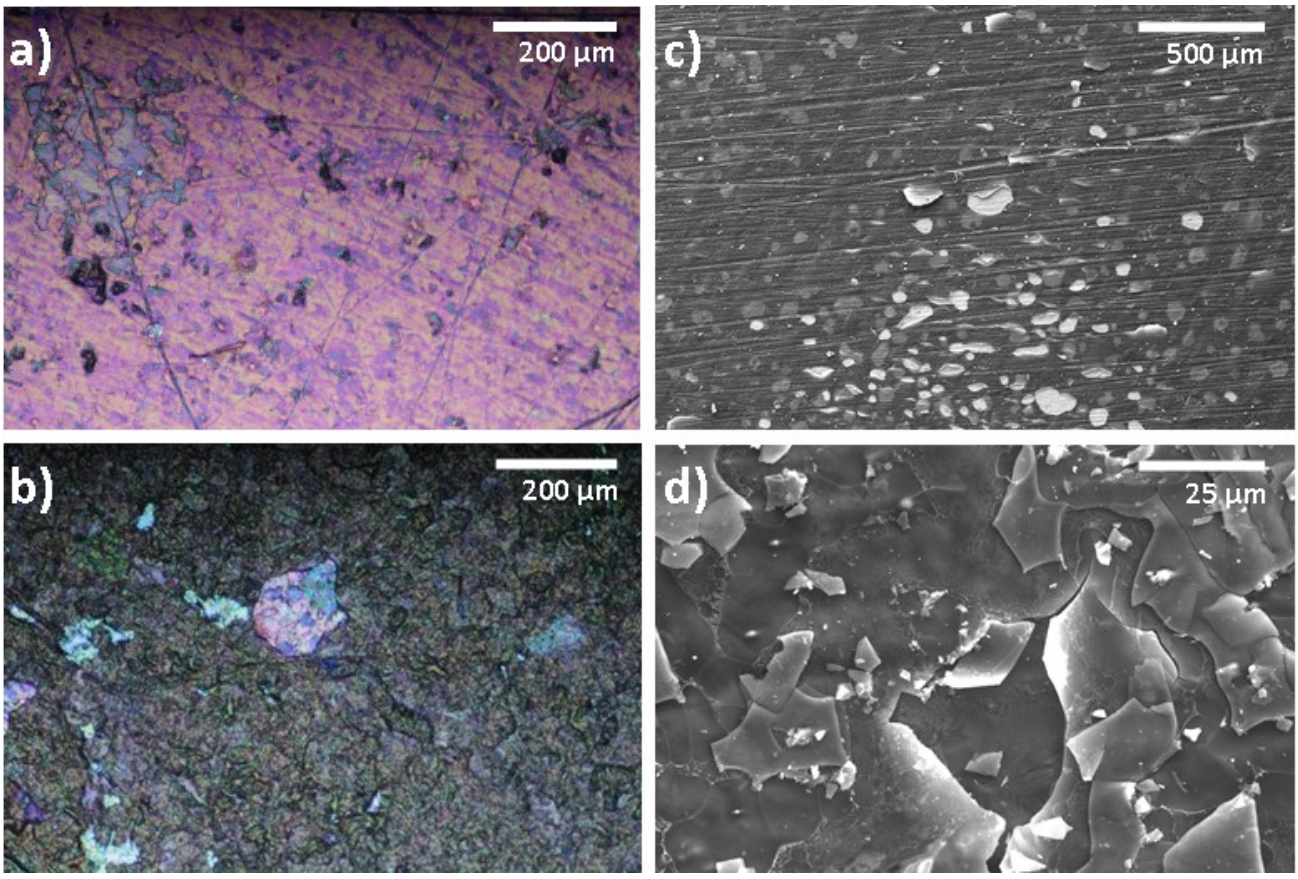

Figure 3: Topological profiles of three profiled regions – a) close to co-NBI with bubbles, b) close to ICRH antenna, c) next to GD antenna.

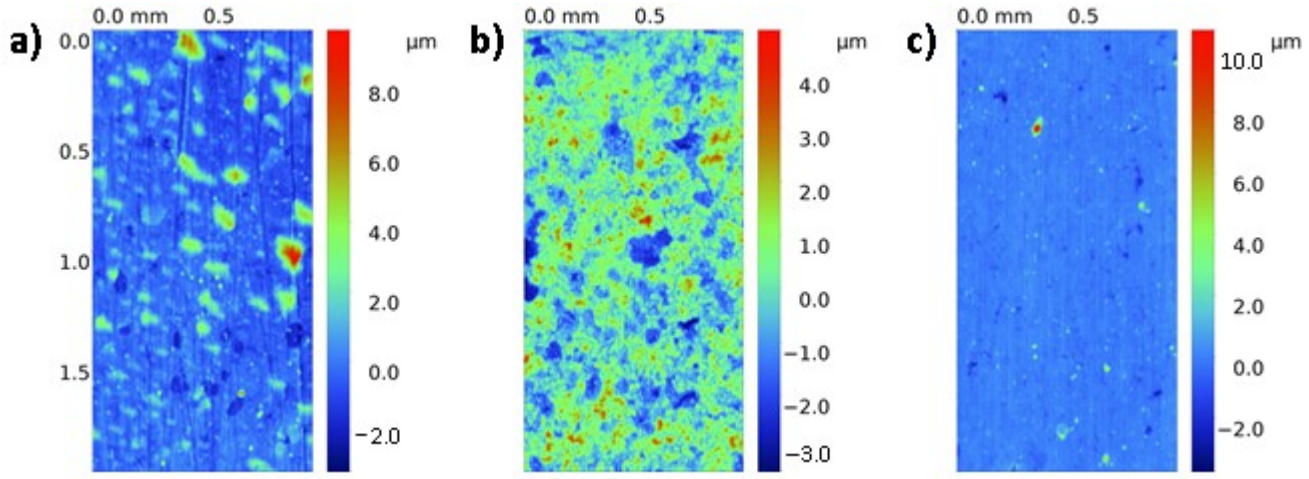

Figure 4: a) ToF ERDA spectrum of the sample next to the GD antenna; b) depth profile for selected elements.

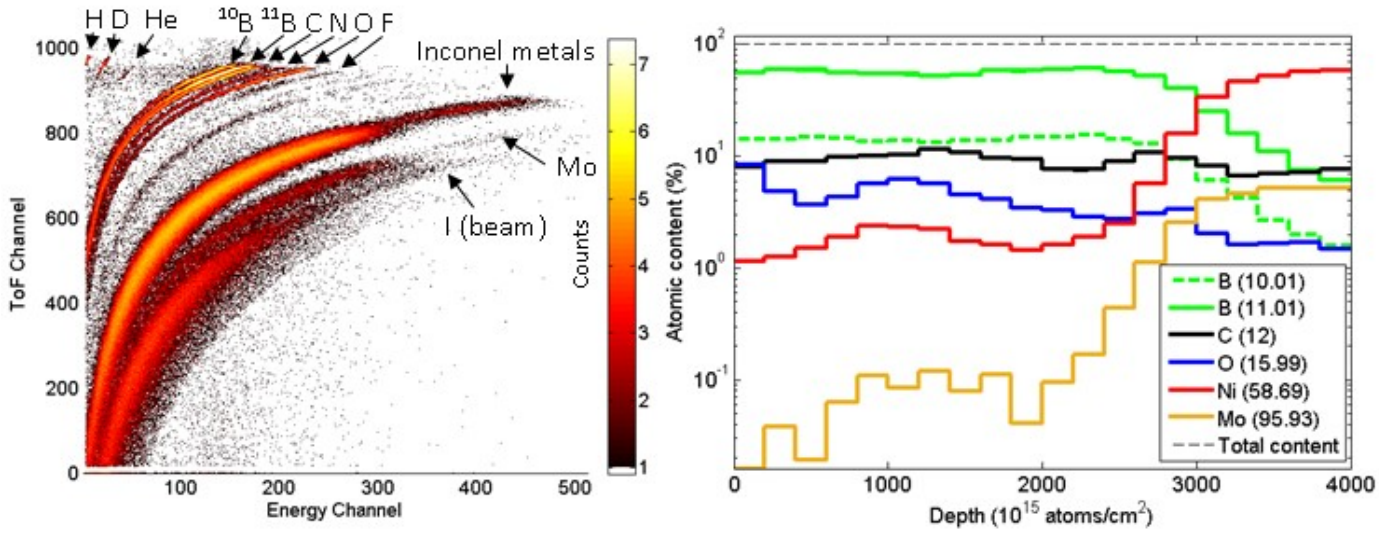

Figure 5: backside of the liner near a) the GD antenna, and b) the co-NBI port.

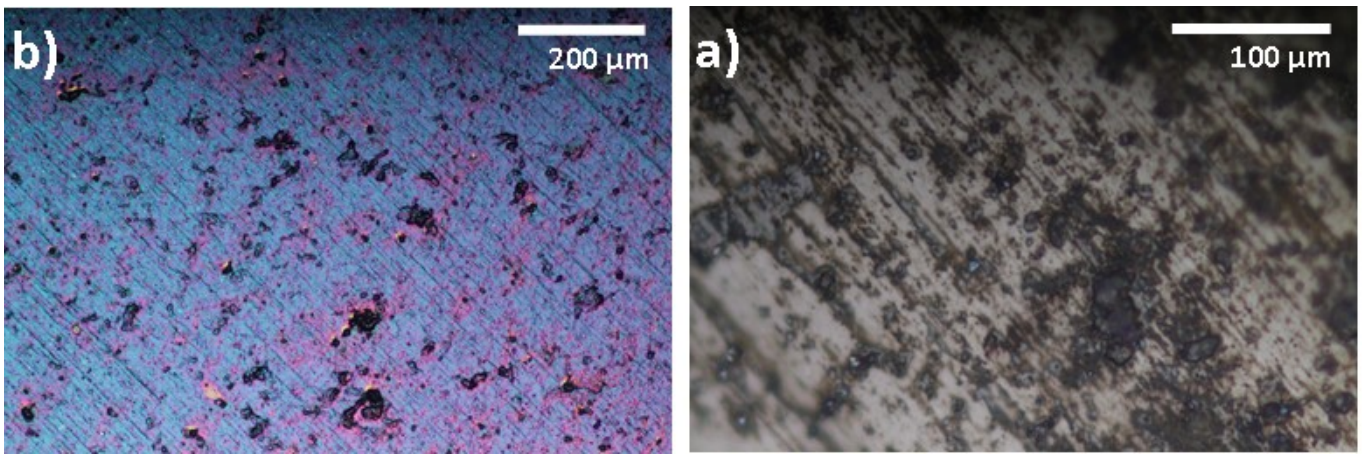

Figure 6: FIB cuts and STEM images for boron, carbon, oxygen and silicon. Other probed elements are omitted.

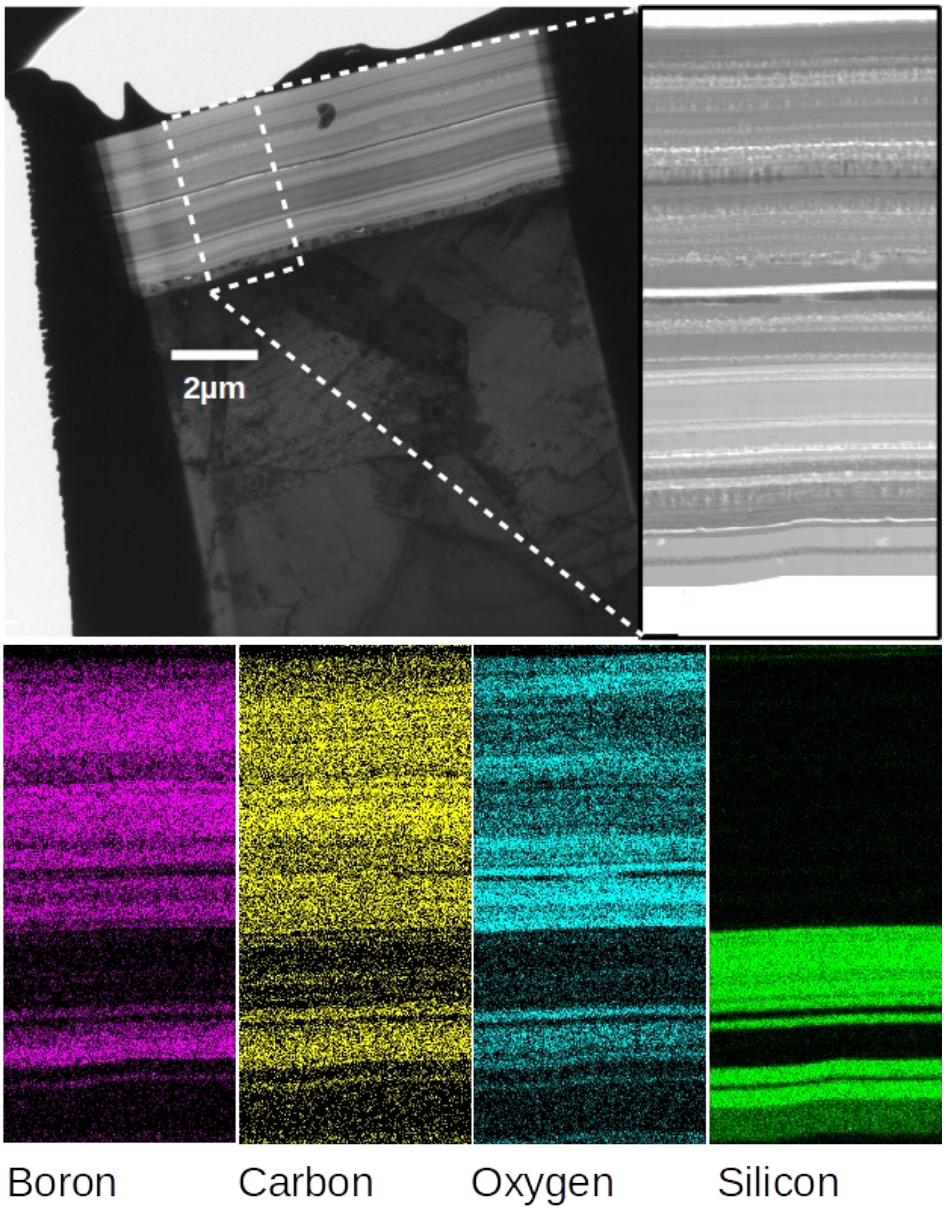

Figure 7: STEM depth profile of elemental maps from Figure 6.

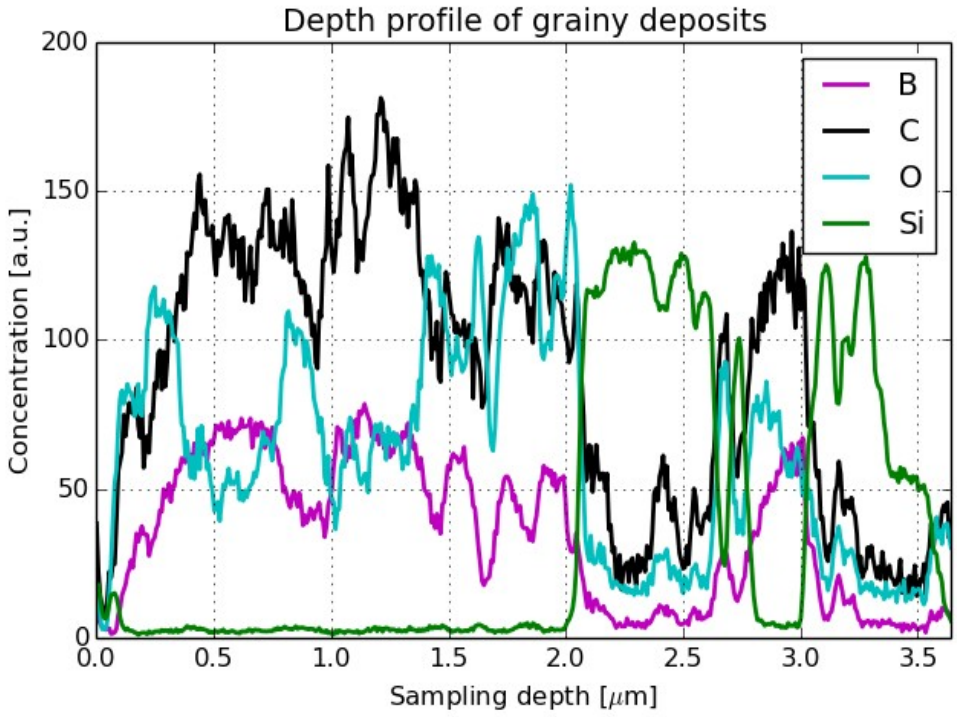

Figure 8: Deuterium depth profiles from all locations, plasma-facing side.